CHRAC/ACF Contribute to the Repressive Ground State of Chromatin

Alessandro Scacchetti[1,2], Laura Brueckner[3#], Dhawal Jain[1,2#], Tamas Schauer[1,2], Xu Zhang[5,6], Frank Schnorrer[5], Bas van Steensel[3], Tobias Straub[4] and Peter B. Becker[1,2*]

[1]Molecular Biology Division, Biomedical Center, Faculty of Medicine, LMU Munich, Germany

[2]Center for Integrated Protein Science Munich (CIPSM), Germany

[3]Division of Gene Regulation, Netherlands Cancer Institute, Amsterdam, The Netherlands

[4]Bioinformatic Unit, Biomedical Center, Faculty of Medicine, LMU Munich, Germany

[5]Developmental Biology Institute of Marseille (IBDM), Aix Marseille Univ, CNRS, France

[6]School of Life Science and Engineering, Foshan University, China

[#] = equal contribution

[*] Correspondence should be addressed to:

Prof. Dr. Peter B. Becker, ML

Division of Molecular Biology
Biomedical Center
Faculty of Medicine, LMU Munich
Großhaderner Strasse 9
82152 Planegg-Martinsried

Tel: +49(0)89-2180-75427

Fax: +49(0)89-2180-75425

Email: pbecker@bmc.med.lmu.de

ABSTRACT

The chromatin remodeling complexes CHRAC and ACF combine the ATPase ISWI with the signature subunit ACF1. These enzymes catalyze well-studied nucleosome sliding reactions *in vitro*, but how their actions affect physiological gene expression is unclear. Here we explored the influence of *Drosophila* CHRAC/ACF on transcription by complementary gain- and loss-of-function approaches.

Targeting ACF1 to multiple reporter genes inserted at many different genomic locations revealed a context-dependent inactivation of poorly transcribed reporters in repressive chromatin. Accordingly, single-embryo transcriptome analysis of a *Acf* knock-out allele showed that only lowly expressed genes are de-repressed in the absence of ACF1. Finally, the nucleosome arrays in *Acf*-deficient chromatin show loss of physiological regularity, particularly in transcriptionally inactive domains.

Taken together our results highlight that ACF1-containing remodeling factors contribute to the establishment of an inactive ground state of the genome through chromatin organization.

INTRODUCTION

The 'Chromatin Accessibility Complex' (CHRAC) and the related 'ATP-utilizing chromatin assembly and remodeling factor' (ACF) are prototypic nucleosome sliding factors purified originally from extracts of *Drosophila* embryos[1,2]. ACF consists of ISWI, an ATPase of the helicase superfamily 2, and a large subunit, ACF1. ACF associates with two histone-fold subunits, CHRAC-14 and CHRAC-16, to form CHRAC[3]. Both complexes have very similar nucleosome sliding activity *in vitro*[4]. Since ISWI is present in several other nucleosome remodelers[5], ACF1 serves as the signature regulatory subunit for the two complexes.

The mechanism of nucleosome sliding has been well described by biochemical and biophysical studies. ISWI and ACF1 bind target nucleosomes and flanking linker DNA. Substrate binding and ATP hydrolysis cycles trigger conformation changes in the remodeler that disrupt

histone-DNA interactions and eventually displace the intact histone octamer along the DNA, effectively sliding a nucleosome[6-12] (for review, see[13]).

Nucleosome sliding may theoretically affect transcription through local and global mechanisms[14]. Locally, nucleosomes could be slid off promoters, exposing binding sites for transcription factors. Conversely, a remodeler might push nucleosomes to occlude regulatory sequences. The yeast Isw2 complex, which is related to the metazoan CHRAC complexes, has been shown to slide nucleosomes towards promoters[15,16]. Alternatively, nucleosome sliding factors may influence transcription by globally affecting the tightness of DNA packaging in chromatin. Nucleosome sliding factors may improve the regularity of nucleosome arrays by closing gaps ('nucleosome spacing'), thus minimizing the level of accessible DNA[1,6,17]. *In vitro*, regularly spaced nucleosome arrays readily fold into '30 nm'-type fibers, a process that has been suggested to promote the formation of 'higher order', repressive chromatin structures[14].

A role for CHRAC/ACF in establishing such repressive chromatin had been derived from early studies of *Acf* mutant embryos that documented defects in nucleosome spacing, in the formation of repressive pericentric heterochromatin and polycomb-mediated silencing[18,19]. A more direct role for ACF1 in the repression of wingless target genes has also been described[20]. The phenotypic oogenesis defects observed in *Acf* mutants[21] may be explained by either mechanism.

These early studies based their conclusions on the analysis of the Acf^{1} allele, that was later shown not to deliver a complete loss-of-function genotype since it still expresses the C-terminal PHD/bromo domains of ACF1[21]. Indeed, some phenotypes observed in Acf^{1} could not be reproduced in a larger gene deletion (Acf^{7}, considered a true null allele) or under RNAi conditions. Therefore, the consequences of a complete loss of ACF1 (and thus the remodeling complexes it defines) are still unknown.

Clues about ACF1 functions at specific loci may be derived from mapping the chromosomal binding sites of the remodeler by chromatin immunoprecipitation (ChIP). Unfortunately, despite many efforts, we were not able to map ACF1 binding sites by ChIP, presumably because the interaction of the remodeler is too transient and dynamic to be efficiently cross-linked[22].

To unequivocally clarify the effect of ACF1-containing remodelers on transcription we performed two key experiments. In a gain-of-function approach we artificially targeted ACF1 to reporter genes integrated at many different chromatin loci and monitored the consequences for reporter gene transcription. Furthermore, using a null allele, we compared the transcriptome of individually staged null mutant to matched wild-type embryos. Both approaches suggest that the main effect of ACF1 on transcription is that it participate to the silencing of genes in inactive chromosomal domains. Importantly, de-repression in mutant embryos correlates with defects in nucleosome spacing. Hence, we conclude that ACF1-containing remodelers contribute to a repressed ground state of the genome through chromatin organization.

RESULTS

Artificial ACF1 tethering leads to context-dependent repression

To investigate potential effects of ACF1 on transcription, we first applied an established approach involving the ectopic targeting of ACF1 to a reporter gene locus. We employed a fly line with a defined genomic insertion of a reporter gene cassette consisting of lacZ/mini-white genes and 5' UAS^{Gal} sequences[23] (**Fig. 1a**). We generated flies expressing N- or C-terminal fusions of ACF1 to the DNA binding domain of the yeast activator GAL4 (GAL4DBD) under the control of the endogenous *Acf* promoter, which assured expression at levels comparable to endogenous ACF1 **(Fig. 1a, b**). A control line harbored a construct expressing only the GAL4DBD. Mating the two types of fly lines yields offspring in which ACF1 is recruited to the UAS^{Gal} element.

Figure 1

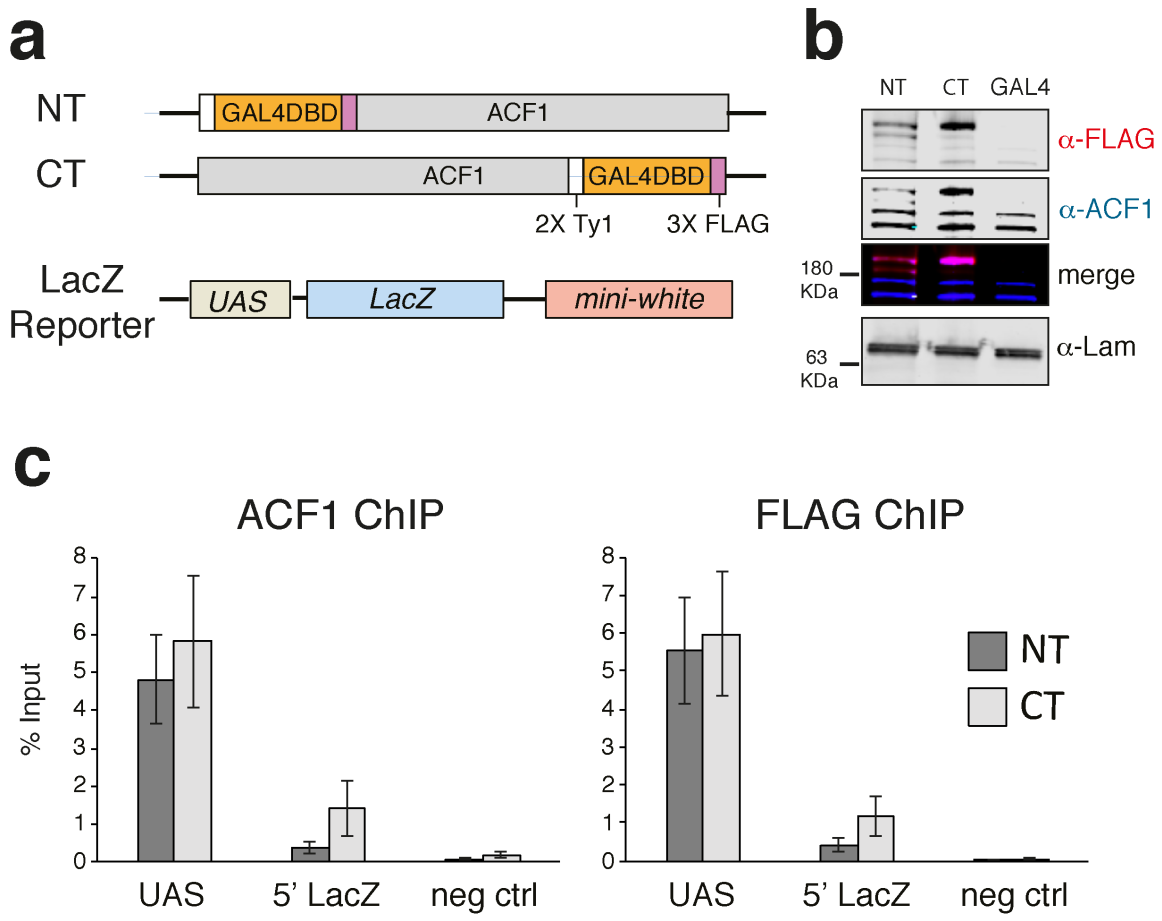

Figure 1. ACF can be tethered to a reporter locus through GAL4-DBD

a. Schematic illustration of the transgenes utilized for testing the effects of ACF1 recruitment. ACF1 is fused to the GAL4 DNA binding domain (GAL4DBD) either at the N-terminus (NT) or the C-terminus (CT). A transgene containing the GAL4DBD alone (GAL4) is used as a negative control. The reporter transgene contains five UAS^{Gal4} (UAS) 5' of *LacZ* and *mini-white* genes.

b. Western blot detection of ACF1 in embryo nuclear extract (0-16 h after egg laying). Endogenous and fusion protein were detected with a specific ACF1 antibody (blue channel), the ACF1-GAL4 fusions are FLAG-tagged and detected with an anti-FLAG antibody (magenta channel). Embryos containing a transgene coding for the GAL4DBD alone (GAL4) is included as a negative control. Lamin serves as loading control.

c. ChIP-qPCR monitors the recruitment of ACF1 to UAS in 0-12h embryos. The IP was conducted using ACF1 and FLAG antibodies. "UAS" and "5' LacZ" denote the regions amplified by qPCR. Bars denote average % Input enrichment (n=3 biological replicates) ± SEM. "neg ctrl" represents a negative control locus (encompassing the *Spt4* gene)

The successful tethering of ACF1-GAL4DBD in early embryos was confirmed by ChIP-qPCR (**Fig. 1c**). The entire remodeler seems to be recruited since its catalytic partner ISWI was also detected at the UAS sites (**Supplementary Fig. S1a**). ACF1 targeting resulted in an about 2-fold reduced *LacZ* transcription relative to the GAL4DBD only (mean fold-change =

0.58 for GAL4DBD-ACF1 and mean fold-change = 0.39 for ACF1-GAL4DBD) (**Supplementary Fig. 1b**). However, no obvious changes in nucleosome positions over and around the reporter locus could be scored by MNase-seq (**Supplementary Fig. 1c,d**).

These experiments provided the proof of principle that a functional ACF1-GAL4DBD fusion protein could be recruited to UAS^{Gal} elements integrated in the fly genome, but it lacked the necessary generalization to document the presumed repressive effect. Therefore, we employed a previously characterized library of several hundred barcoded reporter genes that had been randomly integrated into the genome of *Drosophila* Kc167 cells. We previously tethered the heterochromatin protein 1 (HP1) as a GAL4DBD fusion to these sites and determined how the chromatin environment modulated HP1 repression[24]. HP1, a known repressor, provides a convenient reference for ACF1 in this system. In parallel transient transfections we introduced the various constructs into Kc167 cells and confirmed their expression by Western blotting and immunofluorescence microscopy: GAL4-ACF1, tagged ACF1 lacking a GAL4DBD, ACF1 lacking any tag and a tagged GAL4DBD (**Supplementary Fig. 2a,b,c).**

Like in the case of the single-reporter system, recruitment of ACF1 resulted in a general down-regulation (median log2 fold-change = -1.24), almost comparable to HP1 (median log2 fold-change = -1.46) (**Fig. 2a**), which served as a positive control.

Figure 2

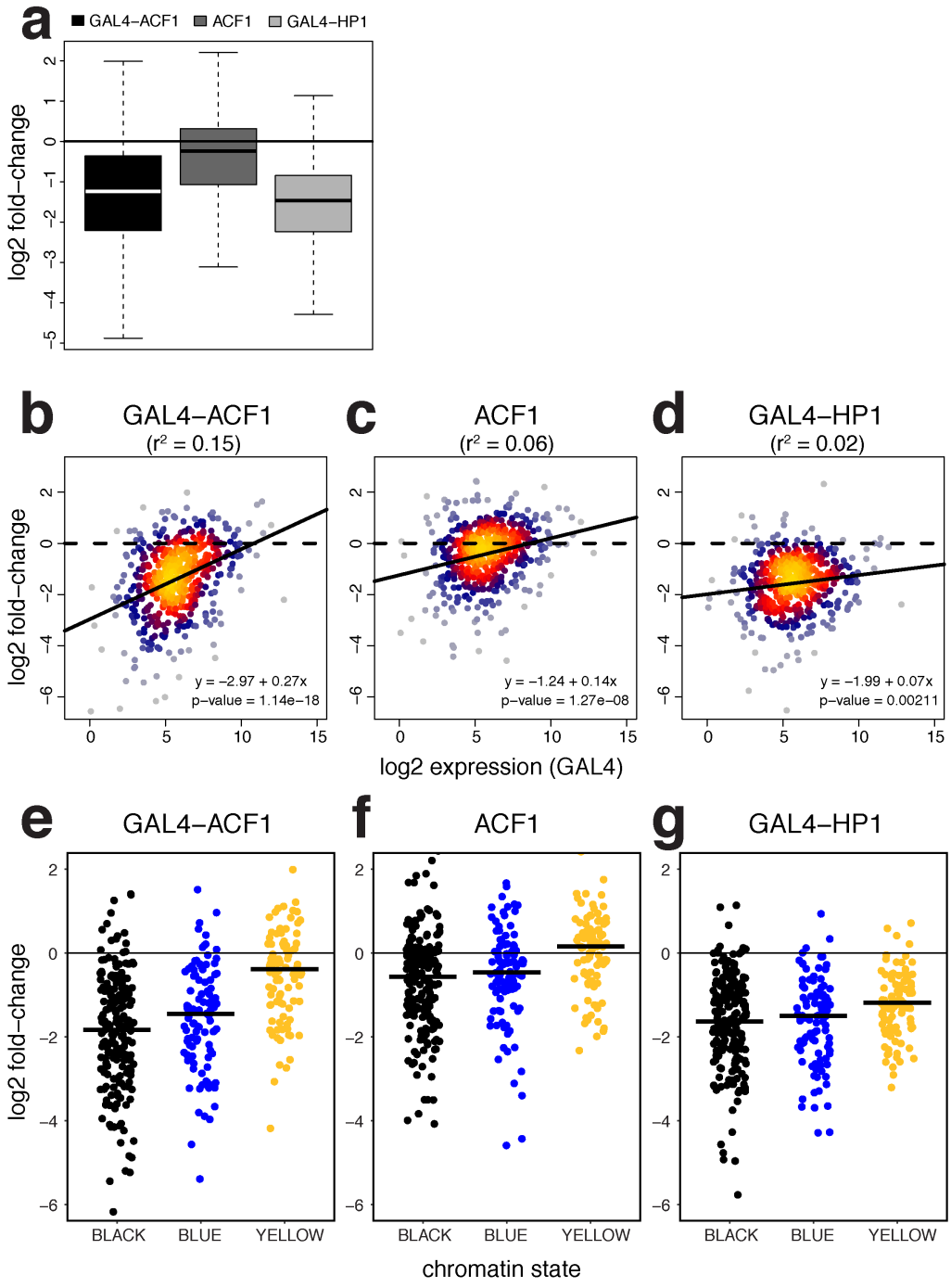

Figure 2. ACF1 represses multiple reporters in a context-dependent manner

a. Boxplots represent log_2 fold-change distribution upon ACF1 tethering (GAL4-ACF1), ACF1 overexpression (ACF1) or HP1 tethering (GAL4-HP1), compared to the control (N = 492).
b. Log_2 fold-change for each reporter in relation to its mean log_2 expression upon ACF1 tethering versus the control (GAL4-ACF1) (N = 492). Black lines represent linear regression fit. r^2 values derived from the linear model are shown in parenthesis. Equation of the regression lines are displayed on the plot. p-value refers to the significance of this relationship (slope).
c. Same as (b) but for ACF1 overexpression (ACF1)
d. Same as (b) but for HP1 tethering (GAL4-HP1).
e. Jitter plot represent the distribution of log2 fold-changes of reporters integrated in BLACK (N = 197), BLUE (N = 102) and YELLOW (N = 94) chromatin domains for the case of tethered ACF1 (GAL4-ACF1). Black horizontal bars represent median.
f. , g. Same as (e) but for ACF1 overexpression (ACF1) and HP1 tethering (GAL4-HP1) respectively

Expression of ACF1 lacking the GAL4DBD had a much weaker effect than its tethered counterpart (median log2 fold-change = -0.24). Interestingly, the extent of ACF1-induced repression inversely correlated with the mean expression levels of the reporters: the repressive effect was less pronounced for reporters with high expression level (**Fig. 2b**). A similar correlation could be also observed for the untethered ACF1 (**Fig. 2c**). The tethered HP1 showed instead just a small correlation between down-regulation and reporter expression (**Fig. 2d**), significantly different from GAL4-ACF1 (**Supplementary Fig. 2d**).

To explore whether the chromatin environment in which the individual reporter genes are integrated modulates ACF1-mediated repression we referred to the 5-state model of chromatin[25]. In this model, YELLOW and RED represent constitutively and developmentally-regulated active chromatin domains, GREEN corresponds to HP1-marked heterochromatic domains, BLACK and BLUE to inactive and polycomb-repressed domains, respectively. We added a sixth state, GREY, to refer to reporters integrated in genomic regions not defined by any of the original 5 states. We found that reporters integrated in BLACK and BLUE chromatin domains are strongly repressed upon ACF1 targeting (BLACK: median log2 fold-change = -1.83, BLUE: median log2 fold-change = -1.45), whereas the ones integrated in YELLOW are only slightly affected (median log2 fold-change = -0.39) (**Fig. 2e).** Similarly, downregulation of reporters in RED (median log2 fold-change = -0.70) and GREEN (median log2 fold-change = -0.97) states results smaller than the one in BLACK and BLUE domains (**Supplementary Fig. 2e**). Recruitment of HP1, instead, shows a more general repressive effect compared to ACF1, which does not correlate with any type of chromatin (**Fig. 2g, Supplementary Fig. 2g**). Interestingly, expression of untethered ACF1 also shows a very mild context-depend repression, reminiscent of its tethered counterpart (**Fig. 2f, Supplementary Fig. 2f**).

In summary, the tethering approach suggested that ACF1-containing remodelers have a repressive function. In contrast to repression by HP1, which served as a positive control for repression, the effect of ACF1 strongly depends on the chromatin context and is particularly robust at lowly expressed genes in overall inactive chromatin domains.

Transcriptome analysis of *Acf*-deficient *Drosophila* embryos

Given the artificial nature of the tethering experiment, we sought to test the hypothesis of a context-dependent repressive effect of ACF1 by a loss-of-function approach in a physiological system. A transcriptome analysis for an ACF1-deficiency has not been reported so far. Conceivably, a function of ACF/CHRAC may be best observed during early embryogenesis in *D. melanogaster* since ACF1 expression peaks during these stages and both, CHRAC and ACF, have been originally identified in embryos. Early on, embryogenesis defects had been noted for the Acf^{1} allele[18]. However, this allele only deletes an N-terminal fragment of the *Acf* gene and still allows expression of a C-terminal 'stub' containing a PHD/bromo domain module that may interfere with relevant interactions. We later concluded that the more extensive deletion of the Acf^{7} allele most likely represents a clean loss of function[21]. In parallel with these earlier studies we generated a clean *Acf* gene deletion employing a CRISPR/Cas9-based engineering approach (Acf^{C}). Expression of ACF1 is not detectable by Western blot in homozygous embryos for the Acf^{C} or Acf^{7} alleles (**Supplementary Fig. 3a;** [21]). Acf^{C} and Acf^{7} embryos show a slightly lower hatching rate compared to their wild-type counterparts (**Supplementary Fig. 3b;** data not shown), but the survivors develop normally into viable and fertile flies (data not shown). We were concerned that Acf^{C} mutants might develop slower than wild-type and hence did not rely on simple developmental stage timing for proper transcriptome comparison. We rather selected single embryos either before zygotic genome activation (ZGA) or after ZGA based on morphological hallmarks (**Fig. 3a,** see methods) and determined their transcriptome by RNA-seq analysis**.**

Figure 3

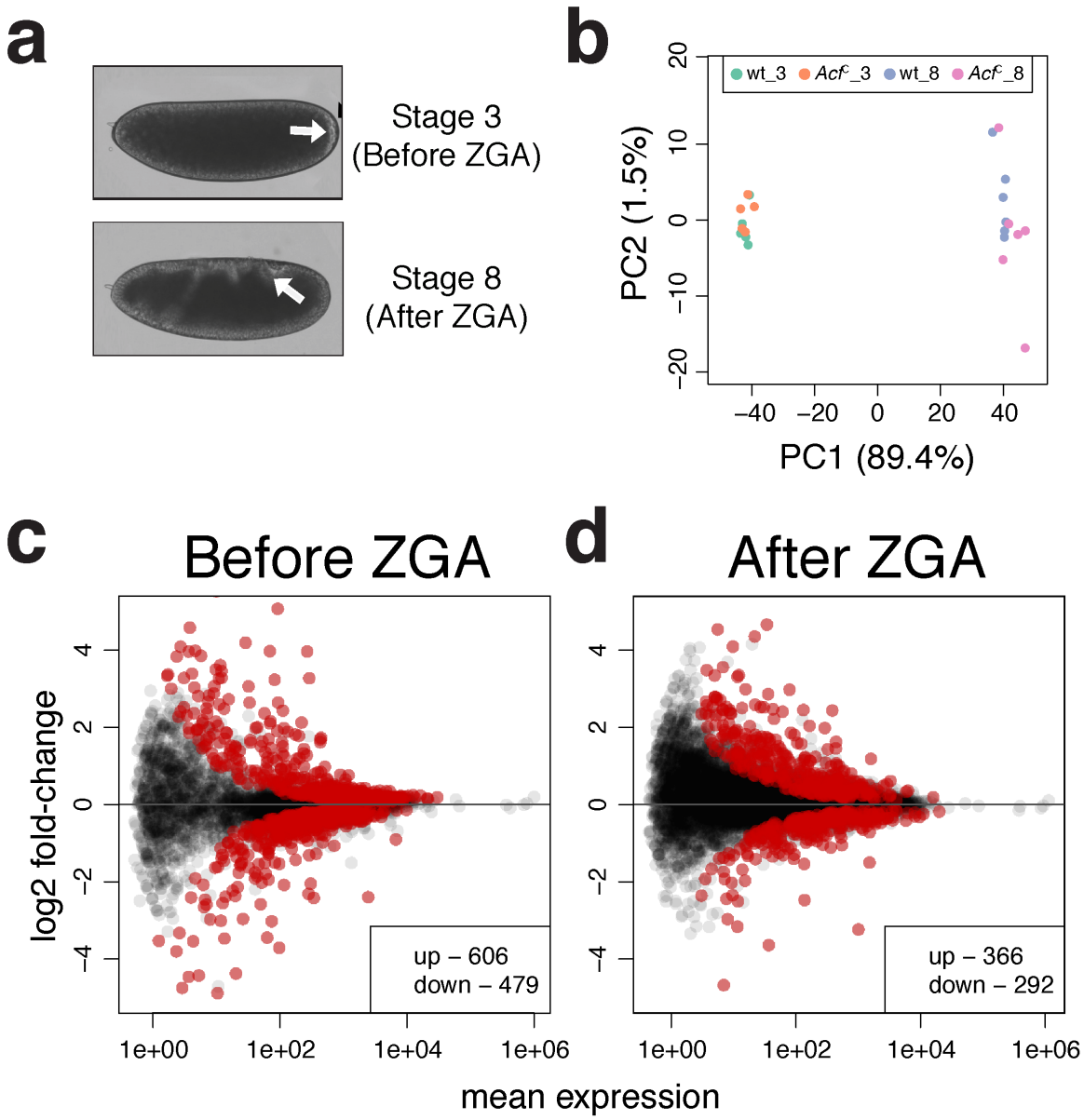

Figure 3. ACF1 loss perturbs gene expression in early embryos

a. Embryo stages selected for transcriptome analysis. In Bownes Stage 3 zygotic transcription is not established yet. Bownes Stage 8 shows robust zygotic transcription. Arrows highlight morphological features of the corresponding stages (appearance of pole cells in Stage 3 and germ band elongation in Stage 8)

b. Principal component analysis (PCA) of single embryos transcriptomes. Each dot represents a single replicate for the corresponding genotype/condition. _3 and _8 indicate embryos before or after zygotic genome activation (ZGA), respectively.

c. Differential gene expression analysis on coding genes from RNA-seq data. *wild-type* and *Acf*^{C} transcriptomes were compared before ZGA (N = 7585). Scatter plots represent $\log_2$ fold-change of *Acf*^{C} over *wild-type* for each gene in relation to its mean expression (mean of normalized counts). Red dots represent significant (q-value <0.1) up- or down- regulated genes.

d. Same as c. but after ZGA (N = 10088).

Principal Component Analysis (PCA) showed no strong differences between *Acf*^{C} and wild-type in both developmental stages (**Fig. 3b**) with clear transition from the maternal to the zygotic RNA pool (**Supplementary Fig. 3c; Supplementary Table 3**). Differential gene expression analysis revealed a relatively small number of genes significantly affected by ACF1 loss at both stages (**Fig. 3c,d; Supplementary Table 2**), but without a clear direction (activation or repression) and without a uniquely defined gene ontology enrichment (**Supplementary Fig. 3d**).

Deletion of the *Acf* gene leads to relaxation of the repressive ground state of chromatin in early embryos

The relatively small number of differentially expressed genes upon *Acf* deletion may be explained by functional redundancy with other remodelers. However, the observation of a context-dependent effects of ACF1 tethering prompted us to relate the transcription effects in embryos to the chromatin state of genes and to their transcriptional activity.

Evaluating the differences between *Acf*^{C} and wild-type embryos in the context of the 5-state model of chromatin organization, we observed a small increase in expression of genes in inactive BLACK and BLUE chromatin domains in *Acf*-deficient embryos. In contrast, genes in the YELLOW domains (**Fig. 4a**) and in GREEN or RED chromatin (**Supplementary Fig. 4a**) were largely unaffected by the loss of ACF1.

Figure 4

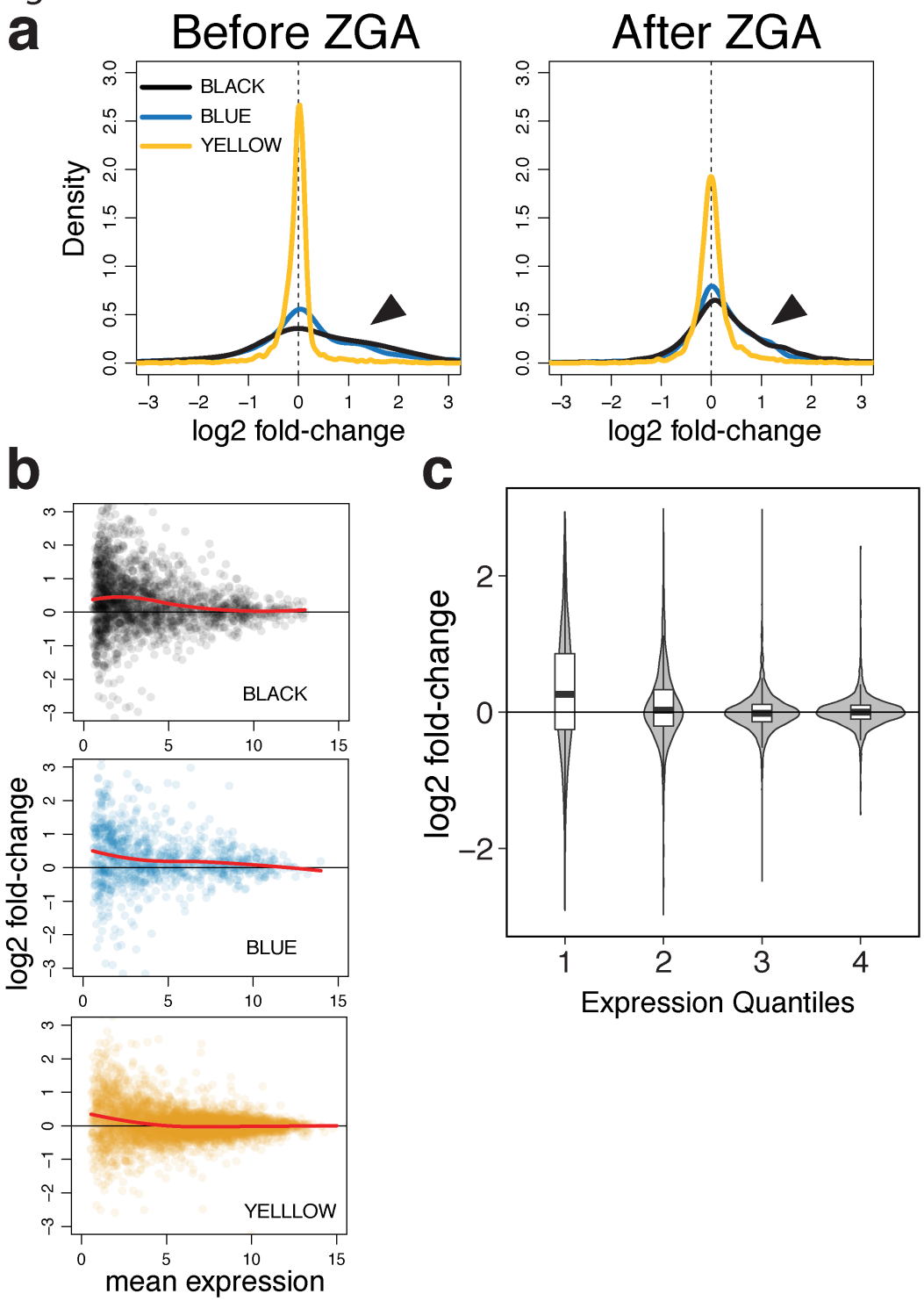

Figure 4. Loss of ACF1 affects transcription prominently in inactive chromatin

a. Comparison of *wild-type* and *Acf*^{C} transcriptomes in relation to the 5-state chromatin model. Graphs represent the distribution of $\log_2$ fold-changes for genes belonging to the YELLOW, BLUE and BLACK chromatin domains before and after ZGA. Arrows indicate the differences between BLACK/BLUE and YELLOW

b. Each scatter plot represents $\log_2$ fold-change for each gene of the indicated chromatin state in relation to its mean expression (after ZGA only). Colors match the chromatin domains as described in the 5-state model. Red lines represent local regression fit.

c. Violin plots represent $\log_2$ fold-change distributions for each given expression quartile (after ZGA only), regardless of chromatin state. Boxplot are overlapped to show median values.

We correlated our data with the modENCODE histone modifications data[26] that had been obtained from 2-4 h embryos, very close to the zygotic stage analyzed in our study. The de-repression of transcription upon ACF1 loss correlates with the absence of defined chromatin marks (BLACK), with the presence of H3K27me3 (BLUE) and with the absence of H3K36me3 (YELLOW) (**Supplementary Fig. 4b**, top panels). No clear correlation was observed for H3K9me3 (GREEN) or H3K4me3 (RED) (**Supplementary Fig. 4b**, bottom panels). The ACF1-dependent effect was most pronounced for lowly expressed genes, not only in the BLACK and BLUE domains, but also in active YELLOW chromatin (**Fig. 4b**). Indeed, the extent of de-repression in *Acf* mutant embryos correlates generally with low expression levels, regardless of the chromatin domain a gene resides in (**Fig. 4c**).

We conclude that loss of ACF1 leads to a widespread de-repression of genes that are characterized by low levels of transcription in wild type. This supports our earlier conclusion derived from the ACF1 tethering experiments.

CHRAC/ACF repress inactive chromatin by maintaining nucleosome regularity

Nucleosome sliding by CHRAC/ACF improves the regularity of nucleosome arrays *in vitro* and hence optimizes the packaging of DNA. Lack of nucleosome spacing activity *in vivo* leads to irregular chromatin, which may explain the observed de-repression phenotype in *Acf* mutants. To test this hypothesis, we analyzed high-quality nucleosome occupancy maps obtained from wild-type and *Acf*^{7} embryos[27] and assessed global chromatin regularity by applying an autocorrelation function to the nucleosome dyad density patterns. Briefly, the function calculates the correlation between nucleosome dyad signals in an array of nucleosomes with a stepwise-shifted copy of itself. The calculated correlation coefficients for each shift (lag) are then plotted as a function of the shift (lag) length. Autocorrelation has previously been applied to score nucleosome repeat lengths[28] and promoter architecture[29]. Applied to nucleosome maps the analysis reveals periodic oscillations, in which the amplitude and the decay rate provide information about regularity, whereas the maxima reveal the distance between

adjacent nucleosomes. For *Acf*^{7} embryos the analysis documents a genome-wide decay of autocorrelation amplitude together with a trend towards increased nucleosome repeat length (wild-type = 188.4 ± 0.7 bp, *Acf*^{7} = 195.3 ± 1.5 bp) (**Fig. 5a**).

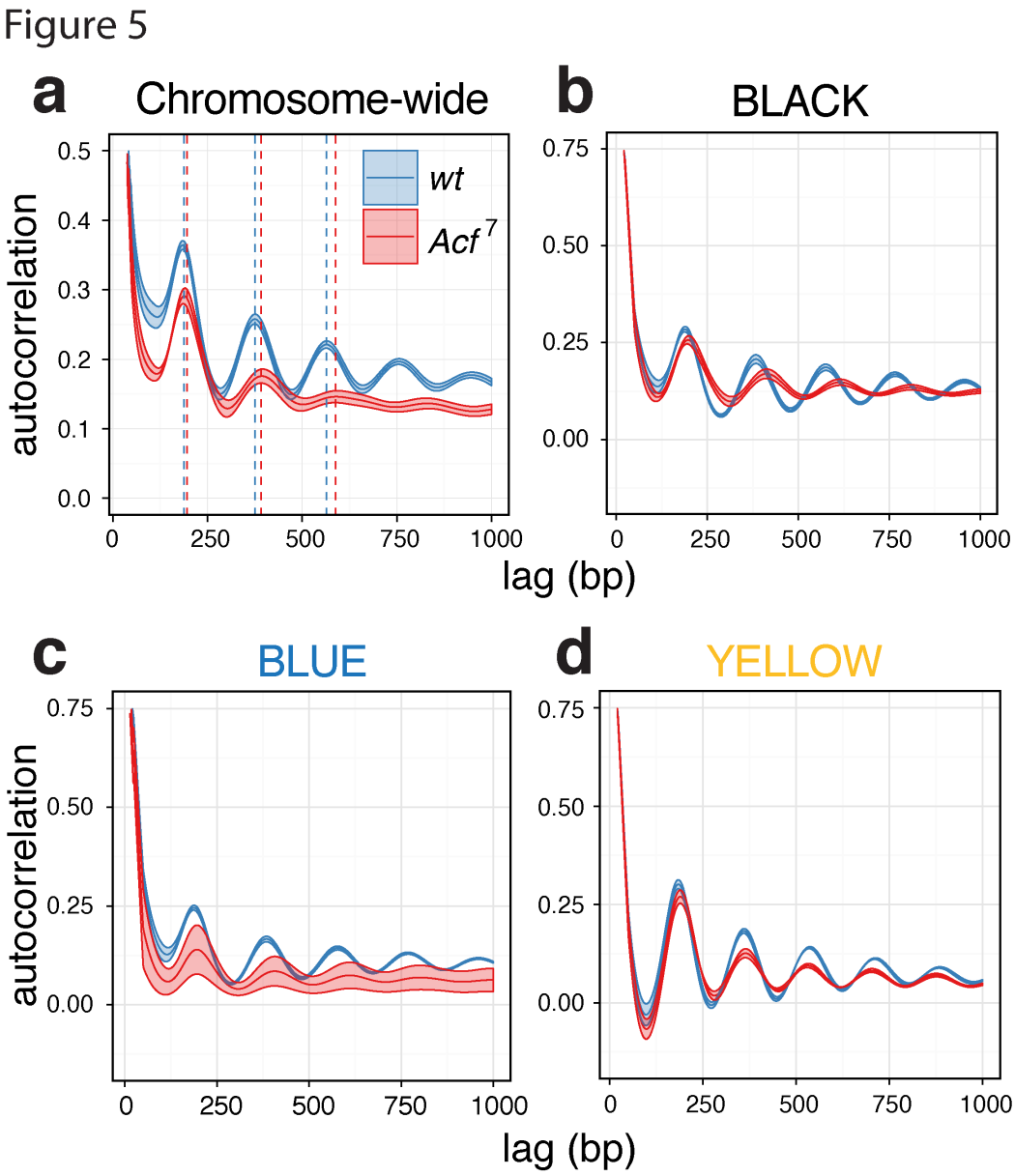

Figure 5. Global and context-dependent decrease in nucleosome regularity as a consequence of ACF1 loss

a. Changes in nucleosome periodicity on chromosomes 2 and 3 are estimated using the autocorrelation function. The correlation coefficients for the nucleosome occupancy values are plotted against the relative shifts (lag). The mean and SEM of replicate samples (n = 5 for *wt* and n=3 for *Acf*^{7}) are displayed. Dashed lines indicate the centers of nucleosome positions derived from the autocorrelation peaks
b. Changes in nucleosome periodicity in BLACK chromatin domains estimated by autocorrelation function. The mean and SEM of replicate samples are displayed.
c. , d. Same as (b) but for BLUE and YELLOW chromatin domains, respectively.

Evidently, loss of ACF1 globally affects the regularity and spacing of nucleosome arrays. To determine whether this global trend applied to the five chromatin states, the autocorrelation

analysis was repeated for each of the chromatin domains. First, we found a dampening of the autocorrelation function upon ACF1 loss in the BLACK and BLUE inactive domains, which was not evident for the YELLOW, active domains (**Fig. 5b-d**). Second, we found a context-dependent increase in nucleosome repeat length in BLACK (*wild-type* = 192.6 ± 0.5 bp, Acf^{7} = 206.0 ± 0.6 bp) and BLUE (*wild-type* = 192.2 ± 0.6 bp, Acf^{7} = 201.0 ± 2.5 bp) but not in YELLOW (*wild-type* = 182.0 ± 0.5 bp, Acf^{7} = 184.0 ± 1.2 bp) domains.

The correlation between the decay of physiological chromatin regularity and de-repression of transcription in *Acf* mutant embryos suggests that the reduced stringency of DNA packaging in the absence of prominent spacing factors perturbs the repressed ground state of the genome installed by nucleosome arrays.

DISCUSSION

The 'Chromatin Accessibility Complex' (CHRAC) was identified two decades ago following a biochemical activity that increased the accessibility of DNA in *in vitro* assembled chromatin[1]. The further characterization revealed that CHRAC did not destroy chromatin, but to the contrary, improved the regularity of nucleosome fibers, identifying a first nucleosome spacing factor. This conundrum was resolved by the discovery that ISWI-containing remodeling factors catalyze nucleosome sliding[6]. ACF, which slides nucleosomes like CHRAC, was originally purified searching for chromatin assembly factors[17,30]. The first genetic analyses of *Acf* deficiencies highlighted defects in pericentric heterochromatin and suppression of variegation, supporting the idea that both 'higher order' chromatin structures and gene silencing rely on proper chromatin organization[18,19]. To this date, however, a systematic assessment of the contribution of ACF1-containing remodelers to transcription has not been done.

Our current study now clarifies this open issue. In our experimental design we avoided several potential pitfalls. (1) We utilized clear *Acf* gene deletion with a clean null phenotype. Previous studies suffered from the fact that the original Acf^{1} allele did not correspond to a null

phenotype, giving rise to unclear gain-of-function effects[21]. (2) To assure that the transcriptome analysis was not flawed by a delay in development of mutant embryos, we hand-selected mutant and wild-type embryos of matched age and determined their transcriptomes individually. (3) We used two orthogonal approaches, each avoiding the technical or conceptual short-comings of the other.

While we could confirm a function of CHRAC/ACF in gene silencing, the extent of transcriptional repression scored in our tethering system was much stronger compared to the one in developing embryos. However, the consequences of the genetic deficiency may be masked by functional redundancy. For example, the ISWI-containing RSF remodeling complex[31,32] possesses similar nucleosome assembly and spacing activities as CHRAC/ACF. The targeting of ACF1 via an ectopic DNA binding domain is expected to locally increase the ACF1 concentration around the tethering site allowing to score effects above the background activities of endogenous factors. Regardless of magnitude, both types of experiments yielded highly complementary results.

The high-throughput targeting system we employed had previously been validated for HP1[24], a well-known repressor, which provided an important benchmark. The repression induced by ACF1 recruitment was of the same order of magnitude as the effect of HP1 tethering determined in parallel. However, the repression mediated by targeted ACF1 was strongly modulated by the chromatin environment, with an obvious effect in overall inactive chromatin domains and lowly expressed genes. This context-dependence of CHRAC/ACF repression was confirmed studying *Acf*-deficient embryos.

Notwithstanding possible functional redundancies, we detected a major and global impact of ACF1 on physiological nucleosome regularity applying autocorrelation function to genome-wide nucleosome dyad maps. The impact of ACF1 depletion was more evident for inactive chromatin domains, establishing a clear correlation between the extent of physiological chromatin regularity and general repression, which we suggest is of causal nature.

Various ISWI-type nucleosome sliding factors have very different functions. NURF[30,33], for example, is recruited by sequence-specific transcription factors to promoters of certain gene classes, where it serves as a co-activator[34]. CHRAC/ACF, in contrast, are most likely not targeted to promoters and enhancers[22]. Conceivably, these remodelers might establish the regularity of the nucleosome fiber in the context of replication[19,35] and/or DNA repair[36,37] and may exert a general 'surveillance' function in search for gaps in the nucleosome array to be closed. We propose that their action establishes a repressive ground state of chromatin, rendering the genome inaccessible through optimal nucleosome packaging. Any further regulation, such as the specific activation of genes by recruitment of histone modifiers and more dedicated remodelers as well as the targeting of silencing machineries, happens on top of the general naïve infrastructure provided by regular nucleosome arrays. CHRAC/ACF and related factors are to be considered the caretakers of this genomic infrastructure. Their important and global role in generating a basal level of genome-wide repression can only be appreciated in regions that are devoid of all other, more potent, targeted and specific regulatory mechanisms.

METHODS

D. melanogaster strains and genetics

The ACF1-GAL4 fusion constructs were generated by recombineering[38]. Briefly, a fosmid containing the genomic region of *Acf* (pflyfos021945) was recombined in *E. coli* with a combinatorial tag cassette consisting of 2x-TY1-GAL4DBD(1-147)-3XFLAG to tag ACF1 either at its N-terminus or its C-terminus, or to entirely replace its coding sequence to serve as a control. Fosmids were inserted into attp40 (*yw*; attP40, locus 25C7, chr2L) (Genetic Services Inc., Boston, MA) to generate fly lines with ACF1 transgenes in chromosome 2L. The mosaic F0 generation was crossed with *w1118* and progeny flies from generation F1 onwards were screened for dsRed phenotype (red eye fluorescence). Homozygous stocks were established by tracking eye fluorescence and the expression of ACF1 constructs was confirmed by Western blotting. ACF1-GAL4 transgenic flies were crossed to N1 flies (Containing the *UAS-LacZ-*

mini-white reporter[23]), to generate the final tethering system.

Generation of the *Acf*^{c} mutant allele

Predicted guide RNAs (sgRNA) targeting sequences for 5' and 3' end of ACF1 were obtained from the Zhang lab CRISPR resource (total 8 for 5' end and 4 for 3' end) (http://crispr.mit.edu/). The 20 bp targeting sequences were inserted into the framework of primer-1 [5'-TAATACGACTCACTATAG-(targeting sequence)-GTTTTAGAGCTAGAAA-TAGC-3'] in 5' to 3' direction. Using scaffold primer (5'-AAAAGCACCGACTCGGTGCCAC-TTTTTCAAGTTGATAACGGACTAGCCTTATTTTAACTTGCTATTTCTAGCTCTAAAAC-3') and universal reverse primer (5'-AAAAGCACCGACTCGGTGCC-3'), a final DNA was as-sembled for *in vitro* transcription by PCR. The PCR product was purified using GeneElute PCR cleanup kit (Sigma, Cat No NA1020). *In vitro* transcription was performed using T7 MEGAshortscript kit (Ambion, Cat No AM1354) and purified RNA was assessed on agarose gel elecrophoresis.

Efficiency of the RNA-mediated cleavage was assessed by transfecting 1 µg sgRNA to 7 x 10^5/ml SL2 cells (clone Hgr14 stably expressing Cas9; [39]) in 2 ml final volume (24 well plate). Genomic DNA was prepared after 48 hr. A ~600 bp region surrounding the selected gRNA sequences was amplified, the PCR product melted at 95°C for 5 min and then cooled slowly with the ramp rate of 0.1°C/sec[40]. gRNA cleavage frequently gives rise to mismatched base pairs around the cutting site, which were detected by T7 endonuclease (M0302S, NEB) cleavage and agarose gel electrophoresis. gRNA combinations that lead to T7 endonuclease cleavage were selected.

Genomic DNA 1.3 kb upstream and 1.5 kb downstream of gRNA sequences for ACF1 were amplified in a high-fidelity PCR reaction. These homology arms excluded the sgRNA sites. The homology arms and 3XP3-dsRed fly selection cassette (obtained from pJet1.2[40]) were assembled together in pBS-donor-backbone by golden gate cloning strategy. The final clone was validated by sequencing.

The purified plasmid and sgRNA for 5' and 3' ends of the *Acf* gene were co-injected into

blastoderm embryos of *yw; Cas9; lig*^{4169} genotype[41]. The F0 mosaic males were crossed with *w1118* females and F1 transformants were screened for red-fluorescence eye phenotype. The flies were backcrossed to *yw* strain for 4 subsequent generations and rendered homozygous. Deletion of the locus was screened by PCR and loss of protein was assessed on WB. Final deletion of ACF1 encompasses around 4 Kb from 562th base onwards removing most of the gene except its 5' and 3' UTRs. For hatching assays, 0-16 h embryos were collected on apple juice agar plates and allowed to develop for additional 25 h at 25°C. Hatched larvae were counted.

Nuclei isolation and Western Blot

For isolation of nuclei, embryos were collected overnight (0-16 h after egg laying [AEL]) onto apple juice agar plates and dechorionated in 25% bleach for 5 min. After extensive washes with PBS (140 mM NaCl, 2.7 mM KCl, 10 mM Na_2HPO_4, 1.8 mM KH_2PO_4), embryos were transferred in 1.5 ml tubes, resuspended in NB-0.3 (15 mM Tris-Cl pH 7.5, 60 mM KCl, 15 mM NaCl, 5 mM $MgCl_2$, 0.1 mM EGTA pH 8, 0.3 M sucrose, 0.2 mM PMSF, 1mM DTT, Roche cOmplete protease inhibitor without EDTA) and homogenized using a metal pestle (LLG Labware, Cat No 9.314.501). The homogenate was collected and carefully layered on top of a bi-phasic solution consisting of NB-1.4 (15 mM Tris-Cl pH 7.5, 60 mM KCl, 15 mM NaCl, 5 mM $MgCl_2$, 0.1 mM EGTA pH 8, 1.4 M sucrose) and NB-0.8 M sucrose. After spinning at 13 krpm for 10 min (4°C), nuclei pellet was collected and washed twice with NB-0.3 (spinning at 5000 rpm for 5 min at 4°C in between washes).

For Western blot analysis, nuclei were suspended in 5X Laemmli Sample Buffer (250 mM Tris-HCl pH 6.8, 10% w/v SDS, 50% v/v Glycerol, 0.1% w/v bromophenol blue, 10% β-mercaptoethanol) and boiled at 96°C for 8 min. The following antibodies were used for Western blots: αACF1 8E3[22] (1:5), αFLAGm2 (1:1000, Sigma, Cat No F1804) and α Lamin T40 (1:1000, kind gift from H. Saumweber).

ChIP-qPCR

For ChIP analysis, embryos were collected 0-12 h AEL and dechorionated in 25% bleach for 3 min. After extensive washes with water, embryos were transferred to 15 ml tubes and weighted. Between 0.5 – 1 g of embryos were washed with 50 ml of PBS/0.01% Triton X-100 and then resuspended in 9 ml of Fixing Solution (50 mM HEPES pH 7.6, 100 mM NaCl, 1 mM EDTA, 0.5 mM EGTA)/3.7% formaldehyde (Merck, Cat No 1040031000). 30 ml of n-Heptane was added and the tubes were shaken for 1 min, following by 13.5 min of incubation on a rotating wheel (18°C). Embryos were pelleted at 3000 rpm for 1 min, resuspended in 50 ml of PBS/0.01% Triton X-100/125 mM glycine and incubated at room temperature (RT) for 5 min. After two washes with PBS/0.01% Triton X-100, embryos were frozen in liquid nitrogen and stored at -80°C until further processing. Frozen embryos were resuspended in 5 ml of RIPA buffer (10 mM Tris-Cl pH 8, 1 mM EDTA, 140 mM NaCl, 1% Triton X-100, 0.1% SDS, 0.1% sodium deoxycholate/1 mM DTT/0.2 mM PMSF/Roche cOmplete Protease inhibitor without EDTA), dounced 10 times using a loose pestle and 10 times with a tight pestle. The homogenate was transferred into a 15 ml tube, spun at 170 g for 10 min at 4°C. Nuclei were resupended in 5 ml of RIPA/g of embryos and split into 1 ml aliquots. Chromatin was soni-cated using a Covaris S220 (100W Peak Power, 20% Duty Factor, 200 Cycles/Burst, 15 min total time) and insoluble material was removed by centrifugation at 13.2 krpm for 20 min (4°C). Soluble chromatin was pre-cleared by adding RIPA-equilibrated 50% slurry of Protein A+G (1:1) sepharose beads and rotating at 4°C for 1h. 200 µl of chromatin was incubated overnight with 4 µl of the respective antibody: αACF1 Rb2[22], αFLAGm2 (Sigma, Cat No F1804) and αISWI Rb1 (Becker Lab, unpublished). 30 µl Protein A+G (1:1) 50% slurry was added and the tubes rotated for 3 h at 4°C. After 5 washes with RIPA buffer, RNase-A was added (10 µg/100 µl, Sigma, Cat. No. R4875) and incubated at 37°C for 20 min. Subsequent protease digestion (using 250 ng/µl Proteinase K, Genaxxon, Cat.no. M3036.0100) and crosslink reversal were performed simultaneously at 68°C for 2 hr. DNA was purified using 1.8X Agencourt AMPure XP beads (Beckman Coulter, Cat No A63880) following standard protocol and eluted in 50 µl of 5 mM Tris-Cl pH 8. Purified DNA was used for standard qPCR analysis at 1:2 dilution. Primers are listed in Supplementary Table 1.

RT-qPCR

For *LacZ* expression analysis, embryos were collected 2-8 h AEL and dechorionated in 25% bleach for 3 min. After extensive washes with PBS, embryos were transferred into a 1.5 ml tube, resuspended in 300 µl of QIAzol (QIAgen, Cat No 79306) and homogenized using a metal pestle. After addition of 700 µl of QIAzol the samples were snap-frozen in liquid nitrogen and stored at -80°C until further processing. RNA was extracted using the standard protocol provided by QIAgen. The Superscript III First Strand Synthesis System (Invitrogen, Cat No 18080051, random hexamer priming) was used to generate cDNA starting from 1.5 µg of total RNA. cDNA was used for standard qPCR analysis at 1:10 dilution. Primers are listed in Supplementary Table 1.

Immunofluorescence microscopy

For immunofluorescence of *D. melanogaster* Kc167 cells, 200 µl of cells (>10^6 cell/ml) were transferred onto poly-lysine coated 3-well depression slides (Thermo Scientific, Cat No 631-0453) and incubated for 1.5 h at 26°C. Cells were washed with PBS and fixed in PBS/3.7% formaldehyde for 10 min. After two washes with PBS, cells were permeabilized in ice-cold PBS/0.25% Triton X-100 for 6 min. Cells were washed twice with PBS and blocked with PBS/0.1% Triton X-100/5% Normal Donkey Serum (NDS, Jackson Immuno Research)/5% non-fat milk for 2 h. After a brief wash with PBS, cells were incubated overnight at RT with primary antibodies αV5 (1:1000, GenScript, Cat No A00623) and αmCherry[42] (1:20). Cells were washed twice with PBS/0.1% Triton X-100 and incubated with secondary antibodies donkey-αrat-Cy3 (1:500, Jackson Immuno Research) and donkey- αrabbit-Alexa488 (1:300, Jackson Immuno Research) for 2 h at RT. Cells were washed twice with PBS/0.1% Triton X-100, incubated with 1:500 DAPI for 10 min at RT and washed again with PBS. Coverslips were mounted using Vectashield Mounting Medium (Vector Laboratories, Cat No H-1000) and sealed with nail polish. Pictures were acquired on a Leica Sp5 confocal microscope using the same settings for all the constructs.

Artificial tethering of ACF1 to multiple reporters in *D. melanogaster* cells

Kc167 cells containing the barcoded reporter library were generated as previously described[24]. Plasmids for the expression of Gal4-ACF1 fusion and controls were derived from pAc5-Gal4-V5-HP1a-T2A-mCherry[24] by Gibson assembly. All constructs were validated using DNA sequencing and restriction digestion analysis. The artificial tethering, including sample preparation, sequencing and data processing/analysis was performed as described in[24], including Gal4-HP1 construct as a positive control. Two biological replicates for each condition were analyzed. Reporters with normalized counts equal to zero in at least one condition were discarded. Linear models were calculated using the *lm* function in R. For transient expression of Gal4-ACF1 fusion and controls, $3x10^6$ Kc167 cells were transfected with 1 µg of the corresponding plasmid using X-tremeGENE HP Transfection Reagent (SIGMA, Cat No 6366236001) following standard protocol (4.5:1 transfection reagent:DNA ratio). Three days after transfection, 1 ml cells were collected, spun at 800 g for 5 min, resuspended in 20 µl of 5X Laemmli Sample Buffer per 10^6 cells and boiled at 95°C for 10 min.

Single-embryo RNA-seq

Prior to RNA-seq, the *Acf*^{C} flies were backrossed with the wild-type *OrR* strain for 8 generations. Embryos were collected 0-45 min AEL and allowed to develop at 25°C until approximately 30 min before the desired stage (around 1 h for Bownes Stage 3 and 4 h for Bownes Stage 8). Without prior dechorionation, embryos were hand-picked and submerged into a drop of Voltalef 10s halocarbon oil (Lehman and Voss Co.) placed on a microscope slide. After about 5 min, the embryonic structures become visible under the stereomicroscope. Embryos were allowed to develop further under the halocarbon oil until the desired stage. Single embryos were picked and crushed with a 26G needle into 200 µl of Lysis Buffer (supplemented with Proteinase K) from the Agencourt RNAdvance Tissue Kit (Beckman Coulter, Cat No A32645). After the addition of 10 µl of 1:100 ERCC Spike-in RNA mix (Ambion, Cat No 4456740), the samples were incubated at 37°C for 20 min, snap-frozen in liquid nitrogen and stored at -80°C. Total RNA was extracted from the single-embryo homogenate using the

same Agencourt RNAdvance Tissue Kit, following standard protocol but utilizing half of the volumes recommended. The RNA integrity was checked on a Bioanalyzer 2100 (Agilent). Ribosomal RNA depletion was achieved using rRNA Depletion Kit (Human/Mouse/Rat) (New Englands Biolab, Cat No E6310) and the rRNA-depleted RNA was stored at -80°C until further processing. Non-directional libraries were prepared using NEBnext Ultra RNA Library Prep Kit for Illumina (New Englands Biolab, Cat No E7530S) following standard protocol. 6 replicates per genotype and stage were sequenced on an Illumina HiSeq1500 instrument. Paired-end RNA-seq reads were mapped against the reference genome (FB2016_01 dmel_r6.09 with selected chromosomes) using STAR (version 2.5.0a) with *quantMode GeneCounts* for counting reads per gene[43]. One replicate from the Acf^{C} genotype (Stage 3) was excluded due to improper staging (data not shown). Size-factors for normalization were calculated by DESeq2[44]. Principal component analysis was carried out on selected genes which variance across samples lies between the 85th and 99th percentile. Genes with a read count equal to zero in at least half of the samples were filtered out for further analysis. Differential expression (DESeq2) analysis (mutant vs. wild-type) was carried out by fitting negative binomial GLM independently for the two developmental stages[44]. Cut-offs for adjusted p-values were defined at the 0.1 level. Full lists of differentially expressed genes are reported in Supplementary Table 2 and Supplementary Table 3. Gene ontology analysis on significantly different genes was performed on the FlyMine online database[45]. Genes were assigned to 5-state chromatin domains[25] by the *nearest* method from the GenomicRanges Bioconductor packages. Trends on MA-plot were visualized by local polynomial regression fitting (*loess*). modENCODE histone modification signals (smoothed M-values)[26] were averaged over genes and low/high levels were distinguished by a cutoff based on the local minimum in the density of the H3K36me3 levels. Genes were classified to marked/unmarked whether they carry high histone modification levels in all four marks investigated in the analysis.

Nucleosome mapping and autocorrelation

For mapping nucleosomes, embryos were collected 2-8 h AEL. Embryos (between 0.2 and

0.5g per replicate and genotype) were dechorionated and fixed as described in the ChIP-qPCR section.

For nuclei isolation, embryos were slowly thawed and dounced using a glass homogenizer (Schubert, Cat.no. 9164693) with 20 strokes each of the A and B pestles in ice-cold NX-I buffer (15 mM HEPES pH 7.6, 10 mM KCl, 2 mM MgCl2, 0.5 mM EGTA, 0.1 mM EDTA, 350 mM sucrose, 1 mM DTT, 0.2 mM PMSF, Roche cOmplete Protease inhibitor without EDTA). Nuclei were subsequently pelleted at 3,500 rpm, 10 min at 4°C. For MNase digestion, the nuclei were suspended in the RIPA buffer supplemented with 2 mM $CaCl_2$. Nuclei were digested with 13 units of MNase per g of starting embryos (Sigma, Cat.no N5386) for 15 min, 37°C while shaking at 500 rpm. The reaction was stopped by adding 0.5 M EDTA (pH 8.0) to a final concentration of 10 mM and the tubes were quickly transferred to ice for 5 min. Nuclei were spun at 12.5 krpm, 10 min at 4°C. The supernatants containing most of the DNA were collected and the residual RNA was digested by RNase-A (50 µg/ml, Sigma, Cat. No. R4875) at 37°C for 30 min. Protein digestion and crosslinking reversal were performed as previously described. DNA was purified using 1.8X Agencourt AMPure XP beads (Beckman Coulter, Cat No A63880) following standard protocol and eluted in 50 µl of 5 mM Tris-Cl pH 8. Recovered DNA was quantified using the Qubit® dsDNA HS Assay Kit (Life Technologies, Cat.no.Q32851) and sequencing libraries were prepared using a custom-made protocol available upon request. Libraries were sequenced on a HiSeq 1500 (Illumina) instrument. Paired-end reads were mapped to *D. melanogaster* genome version dm6. We used Bowtie v1.1.1 with "-X 750" parameter setting. Dyad coverage vectors were obtained by size-selecting fragments of length >120 and <200 bp and resizing their length to 50 bp fixed at the fragment center.

The nucleosome dyad maps used for autocorrelation were generated, validated and interpreted by Jain et al.[27]. The autocorrelation function was calculated for the dyad coverage vectors obtained for the entire genome and for the 5-state domains described by Filion et al[25]. The vectors for the last cases represent head-to-tail concatemerized regions of given annotation. The function was run for the lag length of 1000 bp. Nucleosomal repeat lengths

(NRL) were obtained by linear regression of the first and second autocorrelation peak position with zero intercept. The slope of the regression was defined as repeat length. Values reported in the text correspond to average NRL (between biological replicates) ± SEM.

Accession Codes

Sequencing data have been deposited in the Gene Expression Omnibus under accession numbers GSE106759 (Artificial tethering of ACF1 in Kc167 cells) and GSE106733 (Nucleosome maps and single-embryo RNA-seq)

AKNOWLEDGMENT

We thank K. Förstemann for sharing reagents and cell lines for gRNA testing. We thank S. Krebs and H. Blum and the NKI Genomics Core Facility for outstanding sequencing service. P.B.B. and A.S. are funded by the European Research Council (ERC), MSCA-ITN-2014-ETN No. 642934. F.S. is funded by the ERC [(FP/2007-2013); ERC Grant 310939], the CNRS, the excellence initiative Aix-Marseille University AMIDEX, the ANR and the LabEX-INFORM. B.v.S. is supported by the National Institutes of Health grant U54 DK107965.

AUTHOR CONTRIBUTIONS

A.S. and P.B.B. conceived the project. A.S. and L.B. performed the experiments. D.J. generated the ACF1-GAL4DBD fly lines and the novel *Acf*^{C} mutant (except injections and first screening of the *Acf*^{c} allele which were conducted by X.Z.). L.B. analyzed the data from ACF1 tethering to multiple reporters. T.Sc. performed the analysis of single-embryo RNA-seq. T.St. and D.J. mapped nucleosomes. B.v.S. supervised L.B. and F.S. supervised X.Z.. A.S., D.J., L.B., T.Sc., B.v.S., T.St., and P.B.B. interpreted the data. A.S. and P.B.B. wrote the manuscript with input from all authors.

COMPETING FINANCIAL INTERESTS

The authors declare no competing financial interests.

REFERENCES

1. Varga-Weisz, P.D. et al. Chromatin-remodeling factor CHRAC contains the ATPases ISWI and topoisomerase II. *Nature* **388**, 598-602 (1997).
2. Ito, T. et al. ACF consists of two subunits, Acf1 and ISWI, that function cooperatively in the ATP-dependent catalysis of chromatin assembly. *Genes & Dev* **13**, 1529-1539 (1999).
3. Corona, D.F.V. et al. Two histone fold proteins, CHRAC-14 and CHRAC-16, are developmentally regulated subunits of chromatin accessibility complex (CHRAC). *EMBO J* **19**, 3049-3059 (2000).
4. Hartlepp, K.F. et al. The histone fold subunits of Drosophila CHRAC facilitate nucleosome sliding through dynamic DNA interactions. *Mol Cell Biol* **25**, 9886-96 (2005).
5. Becker, P.B. & Workman, J.L. Nucleosome remodeling and epigenetics. *Cold Spring Harb Perspect Biol* **5**(2013).
6. Längst G., Bonte E.J., Corona D.F.V. & Becker P.B. Nucleosome Movement by CHRAC and ISWI without Disruption or trans-Displacement of the Histone Octamer. *Cell* **97**, 843-852 (1999).
7. Eberharter A. et al. Acf1, the largest subunit of CHRAC, regulates ISWI-induced nucleosome remodelling. *EMBO J* **20**, 3781-3788 (2001).
8. He, X., Fan, H.Y., Narlikar, G.J. & Kingston, R.E. Human ACF1 alters the remodeling strategy of SNF2h. *J Biol Chem* **281**, 28636-47 (2006).
9. Blosser, T.R., Yang, J.G., Stone, M.D., Narlikar, G.J. & Zhuang, X. Dynamics of nucleosome remodelling by individual ACF complexes. *Nature* **462**, 1022-7 (2009).

10. Leonard, J.D. & Narlikar, G.J. A nucleotide-driven switch regulates flanking DNA length sensing by a dimeric chromatin remodeler. *Mol Cell* **57**, 850-9 (2015).
11. Mueller-Planitz, F., Klinker, H. & Becker, P.B. Nucleosome sliding mechanisms: new twists in a looped history. *Nat Struct Mol Biol* **20**, 1026-32 (2013).
12. Racki, L.R. et al. The chromatin remodeller ACF acts as a dimeric motor to space nucleosomes. *Nature* **462**, 1016-21 (2009).
13. Clapier, C.R., Iwasa, J., Cairns, B.R. & Peterson, C.L. Mechanisms of action and regulation of ATP-dependent chromatin-remodelling complexes. *Nat Rev Mol Cell Biol* **18**, 407-422 (2017).
14. Korber, P. & Becker, P.B. Nucleosome dynamics and epigenetic stability. *Essays Biochem* **48**, 63-74 (2010).
15. Fazzio, T.G. & Tsukiyama, T. Chromatin Remodeling In Vivo: Evidence for a Nucleosome Sliding Mechanism. *Mol Cell* **12**, 1333-1340 (2003).
16. Whitehouse, I., Rando, O.J., Delrow, J. & Tsukiyama, T. Chromatin remodelling at promoters suppresses antisense transcription. *Nature* **450**, 1031-5 (2007).
17. Ito, T., Michael, B., Pazin, M.J., Kobayashi, R. & Kadonaga, J.T. ACF, an ISWI-Containing and ATP-Utilizing Chromatin Assembly and Remodeling Factor. *Cell* **90**, 145-155 (1997).
18. Fyodorov, D.V., Blower, M.D., Karpen, G.H. & Kadonaga, J.T. Acf1 confers unique activities to ACF/CHRAC and promotes the formation rather than disruption of chromatin in vivo. *Genes & Dev*, 170-183 (2004).
19. Chioda, M., Vengadasalam, S., Kremmer, E., Eberharter, A. & Becker, P.B. Developmental role for ACF1-containing nucleosome remodellers in chromatin organisation. *Development* **137**, 3513-22 (2010).
20. Liu, Y.I. et al. The chromatin remodelers ISWI and ACF1 directly repress Wingless transcriptional targets. *Dev Biol* **323**, 41-52 (2008).
21. Boerner, K. et al. A role for tuned levels of nucleosome remodeler subunit ACF1 during Drosophila oogenesis. *Dev Biol* **411**, 217-30 (2016).

22. Jain, D., Baldi, S., Zabel, A., Straub, T. & Becker, P.B. Active promoters give rise to false positive 'Phantom Peaks' in ChIP-seq experiments. *Nucleic Acids Res* **43**, 6959-68 (2015).

23. Prestel, M., Feller, C., Straub, T., Mitlohner, H. & Becker, P.B. The activation potential of MOF is constrained for dosage compensation. *Mol Cell* **38**, 815-26 (2010).

24. Brueckner, L., van Arensbergen, J., Akhtar, W., Pagie, L. & van Steensel, B. High-throughput assessment of context-dependent effects of chromatin proteins. *Epigenetics Chromatin* **9**, 43 (2016).

25. Filion, G.J. et al. Systematic protein location mapping reveals five principal chromatin types in Drosophila cells. *Cell* **143**, 212-24 (2010).

26. Celniker, S.E. et al. Unlocking the secrets of the genome. *Nature* **459**, 927-30 (2009).

27. Jain, D., Baldi, S., Zabel, A., Straub, T. & Becker, P.B. Genome-wide analysis of phased nucleosomal arrays revals the functional characteristic of the nucleosome remodeler ACF. *Preprint at* https://www.biorxiv.org/content/early/2016/12/13/093666 (2016).

28. Braunschweig, U., Hogan, G.J., Pagie, L. & van Steensel, B. Histone H1 binding is inhibited by histone variant H3.3. *EMBO J* **28**, 3635-45 (2009).

29. Wan, J., Lin, J., Zack, D.J. & Qian, J. Relating periodicity of nucleosome organization and gene regulation. *Bioinformatics* **25**, 1782-8 (2009).

30. Hamiche A., Sandaltzopoulo R., Gdula, D.A. & Wu, C. ATP-Dependent Histone Octamer Sliding Mediated by the Chromatin Remodeling Complex NURF. *Cell* **97**, 833-842 (1999).

31. LeRoy G., Orphanides G., Lane W.S. & Reinberg D. Requirement of RSF and FACT for transcription of chromatin templates in vitro. *Science* **282**, 1900-4 (1998).

32. Hanai, K., Furuhashi, H., Yamamoto, T., Akasaka, K. & Hirose, S. RSF governs silent chromatin formation via histone H2Av replacement. *PLoS Genet* **4**, e1000011 (2008).

33. Badenhorst, P., Voas, M., Rebay, I. & Wu, C. Biological functions of the ISWI chromatin remodeling complex NURF. *Genes & Dev* **16**, 3186-3198 (2002).

34. Kwon, S.Y., Grisan, V., Jang, B., Herbert, J. & Badenhorst, P. Genome-Wide Mapping Targets of the Metazoan Chromatin Remodeling Factor NURF Reveals Nucleosome Remodeling at Enhancers, Core Promoters and Gene Insulators. *PLoS Genet* **12**, e1005969 (2016).

35. Collins, N. et al. An ACF1-ISWI chromatin-remodeling complex is required for DNA replication through heterochromatin. *Nat Genet* **32**, 627-32 (2002).

36. Sanchez-Molina, S. et al. Role for hACF1 in the G2/M damage checkpoint. *Nucleic Acids Res* **39**, 8445-56 (2011).

37. Lan, L. et al. The ACF1 complex is required for DNA double-strand break repair in human cells. *Mol Cell* **40**, 976-87 (2010).

38. Ejsmont, R.K., Sarov, M., Winkler, S., Lipinski, K.A. & Tomancak, P. A toolkit for high-throughput, cross-species gene engineering in Drosophila. *Nat Methods* **6**, 435-7 (2009).

39. Bottcher, R. et al. Efficient chromosomal gene modification with CRISPR/cas9 and PCR-based homologous recombination donors in cultured Drosophila cells. *Nucleic Acids Res* **42**, e89 (2014).

40. Zhang, X., Ferreira, I.R. & Schnorrer, F. A simple TALEN-based protocol for efficient genome-editing in Drosophila. *Methods* **69**, 32-7 (2014).

41. Zhang, X., Koolhaas, W.H. & Schnorrer, F. A versatile two-step CRISPR- and RMCE-based strategy for efficient genome engineering in Drosophila. *G3 (Bethesda)* **4**, 2409-18 (2014).

42. Rottach, A., Kremmer, E., Nowak, D., Leonhardt, H. & Cardoso, M.C. Generation and characterization of a rat monoclonal antibody specific for multiple red fluorescent proteins. *Hybridoma (Larchmt)* **27**, 337-43 (2008).

43. Dobin, A. et al. STAR: ultrafast universal RNA-seq aligner. *Bioinformatics* **29**, 15-21 (2013).

44. Love, M.I., Huber, W. & Anders, S. Moderated estimation of fold change and dispersion for RNA-seq data with DESeq2. *Genome Biol* **15**, 550 (2014).

45. Lyne, R. et al. FlyMine: an integrated database for Drosophila and Anopheles genomics. *Genome Biol* **8**, R129 (2007).